Available online at www.easd.procedia.org
EASD Procedia EURODYN (2026) 2364-2375

EASD Procedia

EURODYN 2026
XIII International Conference on Structural Dynamics
M. Beer, C. Papadimitriou, H. Jensen, J. Chen, M. Broggi, J. Behrensdorf (eds.)
Hannover, Germany, 27.09.–01.10 2026

RESILIENCE-BASED WIND ASSESSMENT OF AN ARCHETYPAL TALL REINFORCED-CONCRETE BUILDING IN INDIA

Endegena A. Zelelew[1], Chiara Scarapazzi[2], Morowe Mall[1], Aniket Panchal[3], and Anastasia Athanasiou[1]

[1]Bauhaus-Universität Weimar
Weimar, Germany
endegena.ayalew.zelelew@uni-weimar.de

[2]University Mercatorum
Rome, Italy
chiara.scarapazzi@studenti.unimercatorum.it

[3]IIT Gandhinagar
Gandhinagar, India

Keywords: wind, performance-based design, multi-hazard, functionality loss, resilience.

Abstract. *In recent decades, rapid urbanization and rising population density have driven the global growth of tall buildings, making the ability of structures resisting both vertical and lateral loads efficiently a primary design challenge. Performance-based design (PBD) offers an al-ternative to prescriptive codes by targeting specific objectives across varying hazard levels. Performance-based seismic design (PBSD) ensures occupant safety during frequent earth-quakes, structural integrity at design-level earthquakes, and collapse prevention under rare extreme shaking. The ASCE Prestandard for performance-based wind design introduces limit states that allow controlled nonlinearity in the main wind force resisting system thus allowing for knowledge developed in PBSD to be adopted to wind design. To reconcile the conflicting demands of seismic and wind loads, an integrated multi-hazard PBD approach which priori-tizes overall resilience over a single dominant hazard is needed. This study investigates the performance of an archetypal 25-storey reinforced concrete office building representative of modern tall structures on the Indian west coast, a region characterized by a high basic wind speed, 50 m/s, and medium seismicity, PGA = 0.24g. The building, designed according to In-dian standards, is doubly symmetric in plan and regular in elevation and consist of a dual system of shear walls and moment-resisting frames. A detailed 3D model is developed and. evaluated through nonlinear response history analyses in line with FEMA P695 and ASCE standards. Performance objectives and acceptance criteria for wind are mapped to admissible damage states, defined according to the ASCE Prestandard. The resilience of the building is further evaluated by adopting the FEMA P-58 methodology to estimate probabilistic damage, functionality loss, and recovery time. The study demonstrates the potential benefits of perfor-mance-based approaches for tall buildings in high wind regions, while contributing to the broader discourse on wind resilience.*

ISSN:2311-9020 © 2026 The Authors. Published by EASD Procedia.
Peer-review under responsibility of the Organizing Committee of EURODYN 2026.
doi: 10.47964/1326.10833.600

1 INTRODUCTION

The global landscape of urban development has undergone a transformation as accelerated vertical expansion becomes a necessity rather than a choice. This shift towards high-rise construction is driven not only for economic gains but also by the urgent need to house residential, commercial, and infrastructural functions within increasingly dense cities [1]. However, as modern tall buildings evolve to be slenderer and more flexible, the corresponding change in geometry and structural proportion mean their behavior and safety is predominantly governed by lateral loads rather than gravity loads [1, 2]. In line with these shifts, there is a growing emphasis on the performance of the structure beyond mere safety, there is heightened focus on post-event functionality, economic losses, and downtime marking the growing significance of resilience as an alternative to traditional prescriptive design [3–5].

Buildings located in multi-hazard regions have the potential to be subjected to both extreme wind events and severe earthquakes over their operational lifespan [6]. While both hazards are random and dynamic in nature, they trigger different structural responses. Earthquakes are rare, high intensity events that bring about violent, cyclic response over a brief duration, typically lasting less than a minute. To survive such an event, a building must be capable of entering the nonlinear range, utilizing ductility and energy dissipation in order to control structural damage [7, 8]. Conversely, wind represents a frequent and sustained action that can persist for hours. For flexible tall buildings, wind hazards primarily undermine occupant comfort and serviceability requirements, necessitating a stiff structure to fulfill them [4, 9, 10]. This creates a significant conflict during design; a structure designed to be ductile during a seismic event may be far too flexible to satisfy wind induced serviceability requirements, while a structure stiffened to fulfill these wind requirements may inadvertently attract higher seismic forces [6]. Relying on a design philosophy that only considers the dominant hazard can lead to uneconomical structural configurations and hidden vulnerabilities that remain unaddressed [11]. Consequently, there is an evident necessity for a performance-based design (PBD) and ideally resilience-based design (RBD) framework that can integrate these multiple, often competing hazards [11–13].

Performance-based seismic design (PBSD) has transformed tall building design by moving away from prescriptive codes in favor of explicit performance targets such as Immediate Occupancy (IO), Life Safety (LS), and Collapse Prevention (CP) [4]. The formalization of PBSD through the Tall Building Initiative (TBI) guidelines highlighted that standard prescriptive approaches are ill-suited for tall buildings because they fail to account for their unique dynamic behavior [14] [14]. Similarly, performance-based wind design (PBWD) has emerged as a structurally efficient alternative for assessing building behavior under wind events. PBWD places an emphasis on serviceability criteria, comfort limits, while also allowing for controlled limited inelasticity in pre-determined structural members during design level wind events [9, 10].

Despite the individual advancements in PBSD and PBWD, from the significant documents such as ATC 40 [15], FEMA 273 [16] to the recent Prestandards for PBWD [9, 10], multi-hazard PBD remains largely underdeveloped. Current building codes follow designing for one dominant hazard which leads to inconsistent stiffness, ductility, and safety margins across different hazards and a lack of unified performance objectives [17]. Additionally, while fragility curves are advanced and widely used for seismic hazards, multi-hazard fragility functions and vulnerability curves remain to be ana area of minimal investigations that has still not been currently integrated into the assessment of tall buildings [11]. This gap prevents a comprehensive understanding of how the structural demands imposed by one hazard might affect the failure probabilities associated with another hazard, thus preventing a consistent assessment of multi-

hazard vulnerability [12]. While resilience metrics like functionality loss, repair cost, downtime, and recovery pathways are well defined for seismic engineering research, their application within a multi-hazard setting is scarcely examined [4, 5]. These limitations emphasize the necessity for a comprehensive multi-hazard PBD framework that can accurately represent structural responses under realistic seismic, and wind demands while incorporating resilience metrics to enable the assessment of post-event functionality in a multi-hazard context [11–13, 18].

This study tries to address these challenges by introducing a unified multi-hazard PBD framework for tall reinforced concrete buildings. By integrating seismic and wind demands through nonlinear response history analyses (NRHA) and resilience-based metrics, this work moves beyond single hazard PBD. The proposed methodology seeks to provide a coherent approach that jointly evaluates safety, serviceability, and post-event functionality in a multi-hazard environment.

2 METHODOLOGY

Wind and seismic forces stand as the primary hazards impacting structures, historically accounting for similar levels of cumulative damage. However, their frequency differs significantly as while catastrophic earthquakes occur relatively rarely, severe windstorms are a much more frequent occurrence. Table 1 outlines the differences between these two hazards. Seismic events have a short duration, and result in a cyclic loading with a limited number of inelastic excursions. Meanwhile, wind hazards last for a longer duration resulting in a non-zero mean alongwind loading and thousands of inelastic excursions.

Seismic Hazards	Wind Hazards
Short duration	Longer duration
Rare catastrophic events	Frequent severe storms
Cyclic loading	Non-zero mean alongwind loading
Limited number of inelastic excursions	Thousands of inelastic excursions

Table 1: Differences between seismic and wind hazards.

2.1 Multi-hazard performance-based framework

Figure 1 presents the methodology developed herein for the multi-hazard assessment of buildings subjected to both seismic and wind hazards. This framework extends previous work of the last author [18]. Winds and earthquakes can be considered as independent hazards; therefore, the respective assessments can be run in parallel.

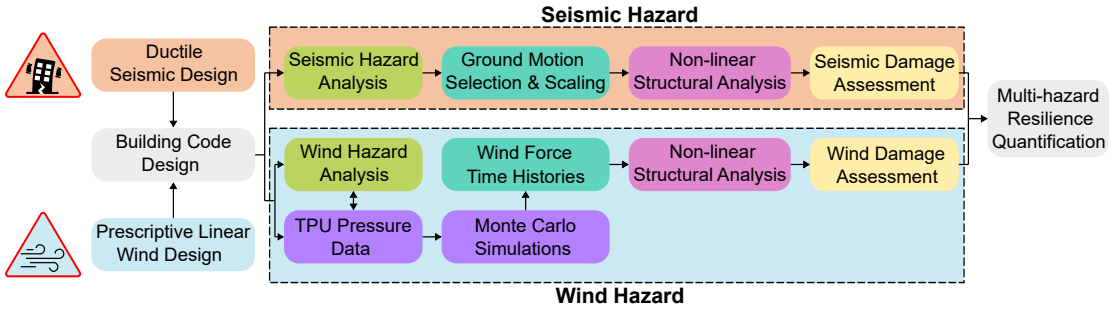


Figure 1: Multi-hazard performance-based assessment framework, including resilience quantification.

The lateral force resisting system (LFRS) is initially designed for gravity and seismic loads, and then the sections are verified for along- , across-, and torsional- wind loads following building codes and standards herein; IS 456:2000 [19]; IS 1893(1):2016 [20]; IS 13920:2016 [21]; IS 875 (3):2015 [22]. The seismic hazard analysis consists in selecting and scaling ground motions to the target response spectrum. A minimum number of 11 ground motions is selected from open-access strong motion databases. The motions are then scaled so that the geometric mean of the response spectra of the selected records matches the site-specific target spectrum. The structural performance is evaluated through a detailed three-dimensional (3D) nonlinear finite element model (FEM), which accounts for material and geometrical nonlinearities, enabling a more accurate assessment of structural behavior under extreme loading conditions through NRHA.

The LFRS performance is assessed at two seismic hazard levels: the Design Basis Earthquake (DBE), corresponding to the life safety limit state, and the Maximum Considered Earthquake (MCE), corresponding to the collapse prevention limit state using far-field ground-motion set available at the ATC database: https://sp3risk.com/ground-motion-sets, see [23]. Limit states are then mapped to acceptance criteria, as shown in Table 2. The resulting Engineering Demand Parameters (EDPs) from the analyses, i.e., interstory (IDR) and residual interstory drifts (RIDR), are then used to assess the performance of the building against the prescribed limits given in Table 2.

Limit State	Performance Level	MRI	Acceptance Criteria	Guidelines
Life Safety (LS)	DBE	475 years	IDR < 0.4%	IS 1893(1): 2016
Collapse Prevention (CP)	MCE	2475 years	IDR < 3% & RIDR < 1%	TBI (PEER, 2017)

Table 2: Seismic limit states and corresponding acceptance criteria.

Wind performance assessment starts by collecting local aerodynamic data of a geometrically similar building (herein wind tunnel data from the Tokyo Polytechnic University (TPU) aerodynamic database: https://db.wind.arch.t-kougei.ac.jp), see [24]. A sufficiently large number (minimum 11) of along-, across- and torsional- wind sets generated through Monte-Carlo simulations are applied on a 3D LFRS model to perform wind NRHA at distinct limits states: Occupant Comfort (OC), Operational (OP) and Continuous Occupancy (CO) following the ASCE Prestandard for PBWD [10], as shown in Table 3. The Collapse Prevention (CP) limit state is introduced to explore response to extreme wind events. Only a single angle of wind attack ($\theta = 0°$, toward the principal X-direction in Figure 2) is considered herein. For square buildings this is expected to provide the most critical responses, at least in the linear range. Peak acceleration (A) and roof drift (DR) responses are then used to assess the wind performance of the building at serviceability and ultimate limit states (SLS and ULS respectively), given in Table 3.

Limit State	Performance Level	MRI	Acceptance Criteria
SLS	Occupant Comfort (OC)	1- and/or 10- years	A < 10-18 milli-g
	Operational (OP)	25-years	DR < 0.2%
ULS	Continuous Occupancy (CO)	700-years	DR < 0.33%, limited yielding
	Collapse Prevention (CP)	1700-years	Moderate inelasticity, no collapse

Table 3: Wind limit states and corresponding acceptance criteria [10].

2.2 Resilience quantification

This study expands on multi-hazard PBD by quantifying the resilience of the components of the main LFRS, i.e. beams, columns, and shear walls, using the methodology proposed in [25]. Resilience, R, is quantified as the normalized area under the functionality curve, $Q(t)$, which is a measure of the ability of the system to maintain or rapidly restore its functionality after an event according to [26]:

$$R = \frac{1}{T_{LC}} \int_{t_{oE}}^{t_{oE}+T_{LC}} Q(t)\,\mathrm{d}t \tag{1}$$

Where, t_{oE} denotes the time of occurrence of the event, TLC defines the control time horizon over which resilience is quantitatively assessed, and the functionality, $Q(t)$, at any post-event moment as defined in [26] is:

$$Q(t) = [1 - L(I, T_{RE})]\,[H(t - t_{oE}) - H\,(t - (t_{oE} + T_{RE}))]\,f_{Rec}(t, t_{oE}, T_{RE}) \tag{2}$$

Where, $L(I, T_{RE})$ denotes the loss function expressed as a function of intensity, I, and time to full recovery, T_{RE}, $f_{Rec}(t, t_{oE}, T_{RE})$ is the recovery function, and $H()$ is the Heaviside step function.

A procedure described in [27] for the calculation of functionality loss and downtime is used in this study. The procedure starts with the assessment of structural damage through the observation of plastic hinge formation. Four distinct plastic rotation ranges, distinct for horizontal (beams) and vertical (columns and shear walls) structural element, are defined and mapped to corresponding damaged states as prescribed in FEMA P-58 [4]. The procedure in [27] then computes functionality loss by associating physical structural degradation to the usage of the building's area. This is done by correlating the degree of observed damage with the fraction of the total floor area that becomes unusable because of that damage. Based on the severity of the damage and the type of structural element affected, functionality loss, FL, is evaluated as:

$$FL(\%) = \frac{A_{\text{non-usable}}}{A_{\text{total}}} \times 100\% \tag{3}$$

Where, $A_{non-usable}$ corresponds to the sum of the tributary areas of all damaged elements, while Atotal denotes the total floor area of the structure [27]. The time period preceding the event is excluded in order to avoid artificially inflating the resilience index. Delay periods right after an event represent a period in which no physical repair work is done, but rescue operations, inspections, fund and permit acquisitions, and mobilization activities take place. These activities are influenced by socio-economic and administrative parameters which can have a high degree of uncertainty. A constant delay period of 30 days is assumed for this study.

The recovery time, TRE, is derived based on data from typical retrofit and repair interventions specific to reinforced concrete structures [25]. Within the multi-hazard framework, the study evaluates resilience to seismic and wind hazards as distinct, separate phenomena. This approach is predicated on the assumption that these two events are statistically independent [18]. A limitation of this framework is using the procedure in [27] with the same modelling assumptions for both wind and earthquake excitation, although the method was not originally formulated to represent these hazards equivalently. This limitation is amplified by the simplification of excluding non-structural components, which often govern post-event functionality especially for wind hazards.

3 CASE STUDY

The case study is a 25-storey office RC building located in an urban environment of the Indian peninsula, and in a particular area of medium seismicity (1-in-475years PGA = 0.12g, medium soil) and strong winds (1-in-50 years basic wind speed U = 50 m/s). The building is doubly symmetric in plan and regular in elevation. Its LFRS consists of a dual system of RC shear walls and moment-resisting frames, as shown in Figure 2. The structure consists of internal beams with cross-sections 0.45 m × 0.60 m and perimeter beams with cross-sections 0.45 m × 0.75 m. The vertical frame members consist of a shear wall, with a 3.6 m × 0.4 m web and 0.6 m × 0.6 m flanges, alongside columns with cross-sections of 0.90 m × 0.90 m for the bottom third, 0.80 m × 0.80 m for the middle third, and 0.70 m × 0.70 m for the top third stories. Excluding the self-weight of the structural members, typical stories have a weight of 8324 kN while the weight at the roof level is 5522 kN.

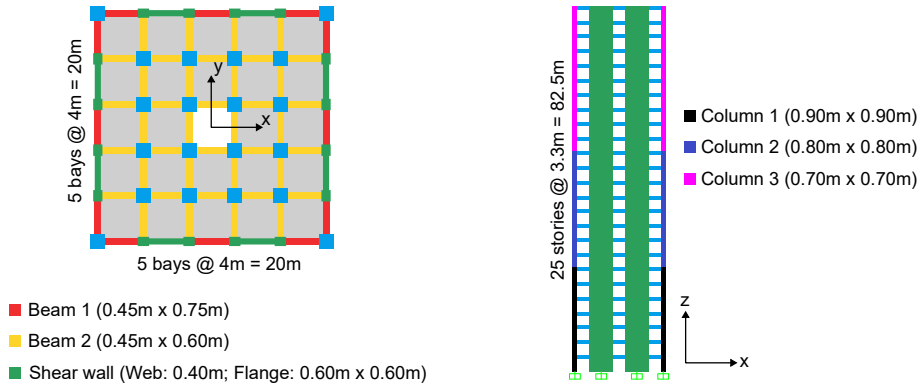


Figure 2: Plan and elevation view of the building with structural member dimensions.

A three-dimensional (3D), nonlinear structural model of the building was developed in SAP2000. The shear wall is modelled using vertical beam-column elements and rigid end offsets applied to the adjoining beams, to replicate the interaction and behavior of a shear wall system and simulate the overall stiffness and lateral load resistance typically provided by a shear wall. The first two modes of the model have a period of 2.82 s and are translational modes in the two orthogonal directions, X and Y, while the third mode is a torsional one with a period of 2.28 s. Rayleh damping calibrated to provide 5% critical damping for the first mode and the mode where cumulative modal mass participation reaches 90% was considered herein.

3.1 Multi-hazard performance assessment

Eleven 3D NRHA were run per limit state and per hazard (seismic and wind) using the spectrum-compatible seismic and wind loadings. Figures 3 and 4 show the mean and the median

peak seismic demands induced by the 475 (DBE) and 2475 (MCE) year earthquakes, expressed in terms of lateral story shear, drift and residual drift in the two main building directions (X and Y). As illustrated by the individual storey shear distributions in Figure 3, the seismic demand is reasonably balanced along the building height and there are no sudden changes in amplitude. The seismic demand follows a similar pattern for both DBE and MCE level demands. IDR results, presented in Figure 4a, demonstrate that the structure satisfies the acceptance criteria of Table 2 for both DBE and MCE. The IDR profiles follow a somehow uniform pattern without abrupt drift concentrations at a single storey. Finally, Figure 4b shows how the obtained RIDR is negligible, peaking at 0.01% for DBE level demands and remaining far below the acceptance criteria for MCE level demands. The results of Figures 3 and 4 point to a stiff RC structure, with moderate excursion to inelasticity under life safety and collapse prevention events. Furthermore, discrepancies in direction dominance of the results can be attributed to the activation of higher modes by some of the ground motions.

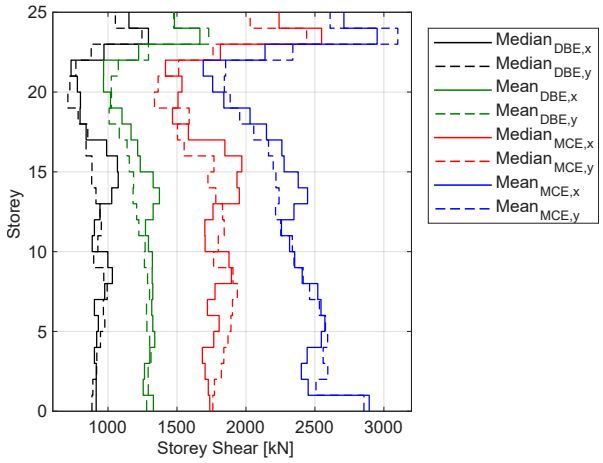
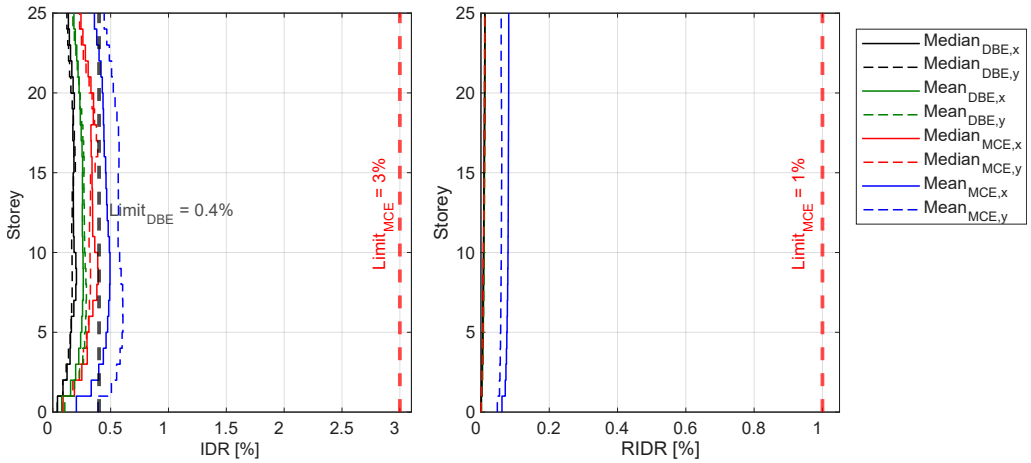


Figure 3: Storey shear distribution under DBE and MCE motions.

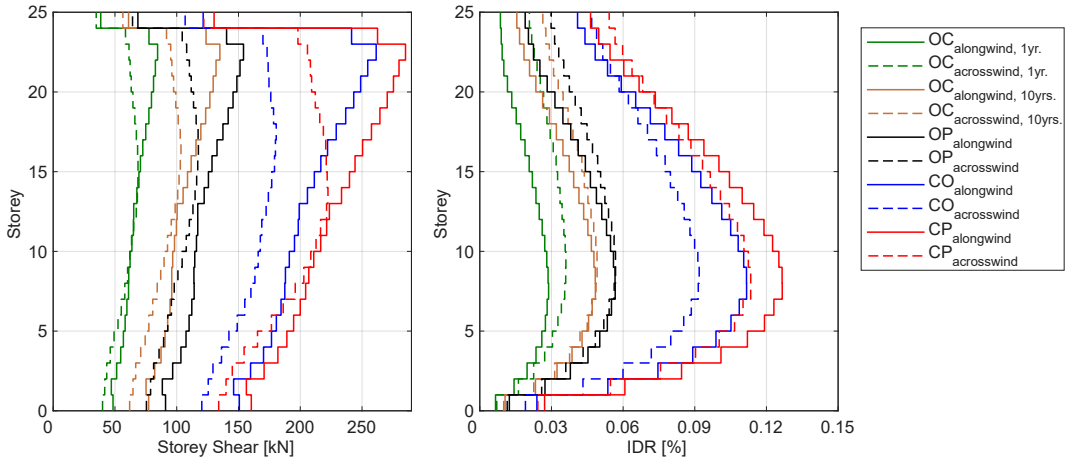


(a) (b)

Figure 4: Directional (a) IDR, and (b) RIDR profiles induced by DBE and MCE motions.

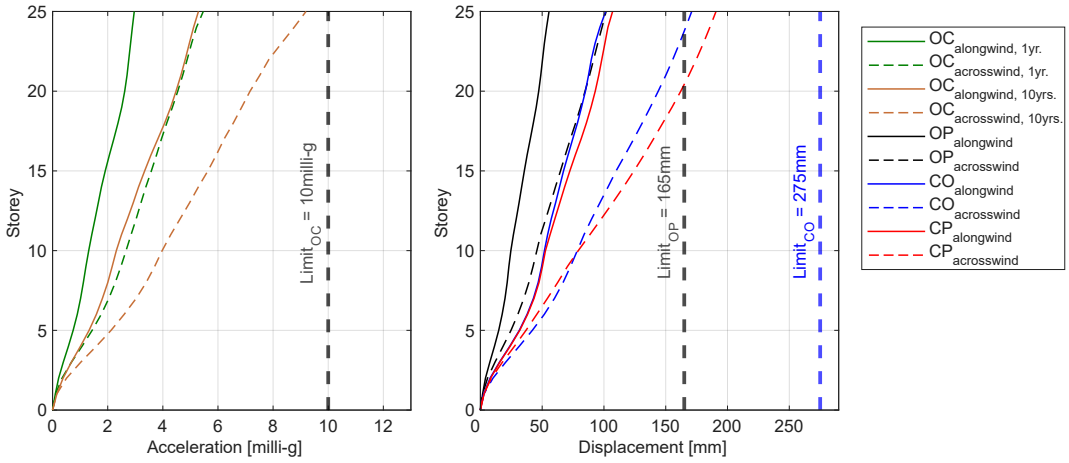
Figures 5 and 6 provide the mean peak response of the office building subjected to 1- (or 10-), 25-, 700- and 1700- year winds, i.e, OC, OP, CO and CP limit states respectively following Table 3. Since the wind-to-wind variability is low, only the mean responses are given herein.

As illustrated in Figure 5a, the wind storey shear increases with building height. Moreover, alongwind storey shears exceed acrosswind ones for both SLS and ULS. However, Figure 5b shows how at SLS, acrosswind IDR exceeds alongwind IDR throughout the whole building height. At ULS the trend changes, alongwind IDRs dominate the response of all floors but the very top ones. The peak floor accelerations presented in Figure 6a show that acrosswind magnitudes are consistently larger than alongwind values at SLS hazard levels and within the acceptance criteria. Finally, Figure 6b provides the corresponding SLS and ULS displacements, which remain within acceptable performance limits, with acrosswind displacements consistently larger than their alongwind counterparts. This suggests that while alongwind effects govern the distribution of force demand along the structure, the deformation response of the structure is driven by acrosswind effects.



(a) (b)

Figure 5: SLS and ULS scaled wind (a) storey shear distribution, and (b) IDR profile.

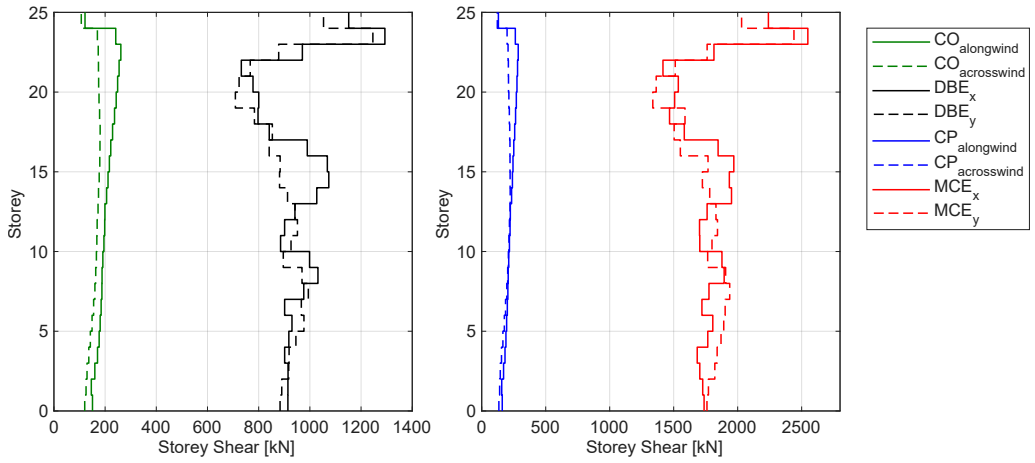


(a) (b)

Figure 6: SLS and ULS scaled wind (a) floor acceleration, and (b) storey displacement.

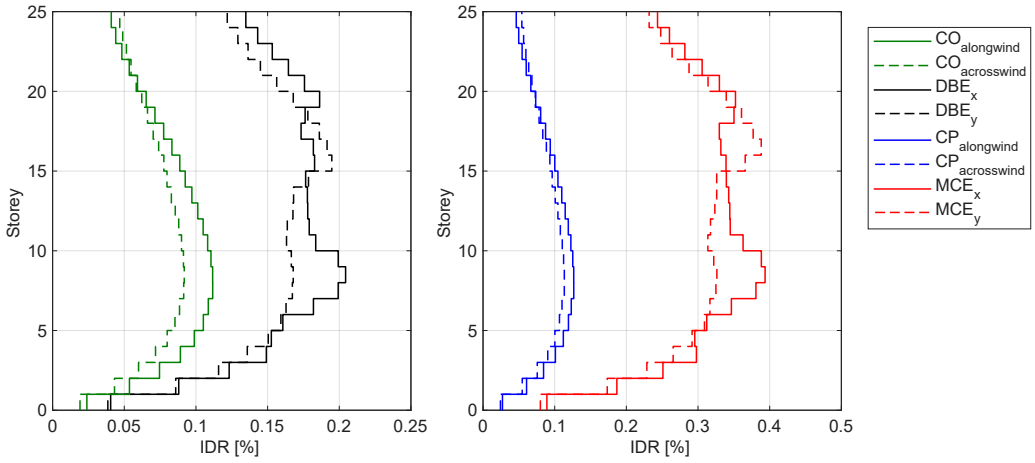
Figures 7 and 8 explore further the differences between seismic- and wind- induced EDPs, by comparing the structural response under DBE (MRI = 475 years) seismic events with CO wind events (MRI = 700 years), and under MCE (MRI = 2475 years) seismic events with CP wind events (MRI = 1700 years). Even though the comparison is not strictly uniform with

matching return periods; these combinations were chosen to investigate structural performance under a multi-hazard scenario. Figure 7 shows that the peak storey shear demand is much higher for earthquake than for wind in both comparison scenarios. Figure 8 illustrates that the inelastic seismic IDR response is significantly higher than the elastic wind IDR response in both scenarios.



(a) (b)

Figure 7: Mean storey shear under (a) DBE and CO wind (b) MCE and CP wind.



(a) (b)

Figure 8: Mean IDR under (a) DBE and CO wind (b) MCE and CP wind.

3.2 Resilience quantification

Figure 9 shows the mean functionality curves for DBE and CP wind events. The two hazards exhibit comparable recovery trends, however the recovery path for the DBE shows a need for an increased repair time. This difference is caused by the slightly more extensive damage caused by the seismic records. The downtime observed under both hazards shows that the structure is unable to achieve rapid recovery leading to a sustained reduction in $Q(t)$. Table 4 shows the functionality loss and resilience index. The increased damage associated with the seismic records is reflected in higher functionality loss and lower resilience index. Following the work of [28], degree of severity of functionality loss is linked to downtime, and given the building's slow recovery capacity the reported functionality loss can be regarded to be high.

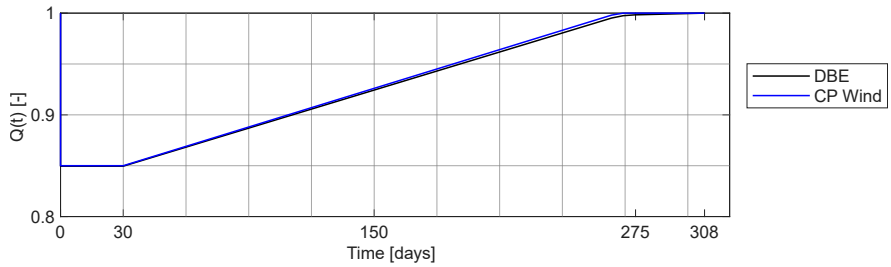


Figure 9: Mean functionality curve for DBE and CP wind.

Hazard	R	FL [%]
Earthquake	0.9671	15.04
Wind	0.9677	15.00

Table 4: Mean values of Resilience index (R) and Functionality Loss (FL) for DBE and CP wind.

4 CONCLUSIONS

This work applied a unified multi-hazard PBD framework capable of consistently assessing the seismic and wind performance of flexible buildings. The framework combines NRHA and FEMA P-58 resilience quantification for both hazards, to evaluate the behaviour of the structure from elastic serviceability to nonlinear response and post-event functionality. Its application to a representative 25 storey RC office building in a region exposed to medium seismicity and high wind demands revealed the advantages of analyzing the two hazards within a single methodological system which provides a more coherent understanding of performance demands than conventional single hazard approaches. The results revealed that no single hazard governs all response parameters. While wind loading governs the displacement profile, seismic excitation governs IDR, and storey shear demands. This illustrates that designing only for a dominant hazard does not necessarily guarantee adequate performance across all EDPs. The results also demonstrate that the relative influence of wind and seismic actions varies with intensity level. For moderate hazard levels (DBE, CO wind), wind effects are the main driver of displacement response, while seismic loading governs IDR and storey shear. However, at extreme hazard levels (MCE, and CP wind), seismic excitation dominates all EDPs, including displacements. These results show that hazard dominance is not constant but evolves with both the hazard intensity and the specific EDP under consideration. The resilience assessment indicates that the building follows comparable functionality trajectories under DBE and CP wind, but its limited recovery capacity leads to relatively high functionality loss. This stresses the need to set recovery focused indicators within multi-hazard frameworks. However, the current approach is limited by the use of an identical procedure for both hazards and by the omission of non-structural elements. Future studies could refine the methodology to differentiate between hazard specific failure mechanisms and to include the effects of non-structural components, thus improving the accuracy of the resilience estimates. This approach is particularly suited to regions characterized by both seismic and wind hazards, where traditional single hazard designs might overlook critical performance indicators. In broad terms, the work contributes to the shift towards resilient, performance-based tall building design by demonstrating the added value of a unified multi-hazard framework. The integration of resilience metrics such as downtime, recovery trajectories, and functionality loss demonstrates how tall buildings can be designed not only to withstand extreme events but also to endure these events and remain operational after an event.

REFERENCES

[1] Ali Mir M. and Kyoung Sun Moon. "Structural Developments in Tall Buildings: Current Trends and Future Prospects". In: *Architectural Science Review* 50.3 (2007), pp. 205–223. DOI: 10.3763/asre.2007.5027.

[2] Ahsan Kareem, Tracy Kijewski, and Yukio Tamura. "Mitigation of motions of tall buildings with specific examples of recent applications". In: *Wind and Structures* 2.3 (1999), pp. 201–251. DOI: 10.12989/WAS.1999.2.3.201.

[3] Michel Bruneau et al. "A Framework to Quantitatively Assess and Enhance the Seismic Resilience of Communities". In: *Earthquake Spectra* 19.4 (2003), pp. 733–752. DOI: 10.1193/1.1623497.

[4] FEMA. *Seismic Performance Assessment of Buildings*. FEMA P-58. Washington, D.C.: Federal Emergency Management Agency, 2018. URL: https://femap58.atcouncil.org/reports (visited on 03/01/2026).

[5] Ibrahim Almufti and Michael Willford. *REDi™ Rating System: Resilience-based Earthquake Design Initiative for the Next Generation of Buildings*. Tech. rep. San Francisco, CA: Arup, 2013. DOI: 10.13140/RG.2.2.20267.75043.

[6] Micol Ciabattoni, Francesco Petrini, and Stefano Pampanin. "Multi-hazard design of low-damage high-rise steel–timber buildings subjected to wind and earthquake loading". In: *Engineering Structures* 303 (2024), p. 117522. DOI: 10.1016/j.engstruct.2024.117522.

[7] Jack P. Moehle and Gregory G. Deierlein. "A framework methodology for performance-based earthquake engineering". In: *Proceedings of the 13th World Conference on Earthquake Engineering (WCEE 2004)*. 2004. URL: https://api.semanticscholar.org/CorpusID:107891620 (visited on 03/01/2026).

[8] ASCE. *Seismic Evaluation and Retrofit of Existing Buildings*. ASCE/SEI 41-17. American Society of Civil Engineers, 2017. DOI: 10.1061/9780784414859.

[9] ASCE. *Prestandard for Performance-Based Wind Design*. American Society of Civil Engineers, 2019. DOI: 10.1061/9780784482186.

[10] ASCE. *Prestandard for Performance-Based Wind Design V1.1*. American Society of Civil Engineers, 2023. DOI: 10.1061/9780784484739.

[11] Anastasia Athanasiou et al. "Multihazard Performance-Based Assessment Framework for Multistory Steel Buildings". In: *Journal of Structural Engineering* 148.6 (2022), p. 04022054. DOI: 10.1061/(ASCE)ST.1943-541X.0003331.

[12] Mingfeng Huang. *High-Rise Buildings under Multi-Hazard Environment*. 1st ed. Singapore: Springer Singapore, 2017. ISBN: 978-981-10-1743-8. DOI: 10.1007/978-981-10-1744-5.

[13] Maria Koliou et al. "State of the research in community resilience: progress and challenges". In: *Sustainable and Resilient Infrastructure* 5.3 (2020), pp. 131–151. DOI: 10.1080/23789689.2017.1418547.

[14] PEER. *Report No. 2017/06 - Guidelines for Performance-Based Seismic Design of Tall Buildings*. Version 2.03. University of California, Berkeley: Pacific Earthquake Engineering Research Center, 2017. URL: https://peer.berkeley.edu/research/building-systems/tall-buildings-initiative (visited on 03/01/2026).

[15] ATC. *Seismic Evaluation and Retrofit of Concrete Buildings*. ATC-40. Redwood City: Applied Technology Council, 1996.

[16] FEMA. *NEHRP Guidelines for the Seismic Rehabilitation of Buildings*. FEMA-273. Washington, D.C.: Federal Emergency Management Agency, 1997.

[17] ASCE. *Minimum Design Loads and Associated Criteria for Buildings and Other Structures*. ASCE/SEI 7-22. American Society of Civil Engineers, 2021. DOI: 10.1061/9780784415788.

[18] Anastasia Athanasiou, Lucia Tirca, and Ted Stathopoulos. "Nonlinear Wind and Earthquake Loads on Tall Steel-Braced Frame Buildings". In: *Journal of Structural Engineering* 148.8 (2022), p. 04022098. DOI: 10.1061/(ASCE)ST.1943-541X.0003375.

[19] BIS. *Plain and reinforced concrete - code of practice*. IS 456:2000. New Delhi: Bureau of Indian Standards, 2000.

[20] BIS. *Criteria for earthquake resistant design of structures, Part 1: General provisions and buildings*. IS 1893 (Part 1):2016. New Delhi: Bureau of Indian Standards, 2016.

[21] BIS. *Ductile design and detailing of reinforced concrete structures subjected to seismic forces - code of practice*. IS 13920:2016. New Delhi: Bureau of Indian Standards, 2016.

[22] BIS. *Design loads (other than earthquake) for buildings and structures - code of practice, Part 3: Wind loads*. IS 875 (Part 3): 2015. New Delhi: Bureau of Indian Standards, 2015.

[23] Haselton Baker Risk Group. *Seismic Performance Prediction Platform*. online. 2026. URL: https://sp3risk.com/ground-motion-sets/ (visited on 02/01/2026).

[24] Tokyo Polytechnic University. *TPU Aerodynamic Database*. online. 2026. URL: https://db.wind.arch.t-kougei.ac.jp/ (visited on 02/01/2026).

[25] Carlos González, Mauro Niño, and Gustavo Ayala. "Functionality Loss and Recovery Time Models for Structural Elements, Non-Structural Components, and Delay Times to Estimate the Seismic Resilience of Mexican School Buildings". In: *Buildings* 13.6 (2023), p. 1498. DOI: 10.3390/buildings13061498.

[26] Gian Paolo Cimellaro, Andrei M. Reinhorn, and Michel Bruneau. "Framework for analytical quantification of disaster resilience". In: *Engineering Structures* 32.11 (2010), pp. 3639–3649. DOI: 10.1016/j.engstruct.2010.08.008.

[27] Ramírez-Herrera and Lugo. *Effects of the earthquake (7.0=Mw) that occurred on June 15, 1999 in Puebla and neighboring States*. Invest. Geog., 2000.

[28] Melissa De Iuliis et al. "Downtime estimation of building structures using fuzzy logic". In: *International Journal of Disaster Risk Reduction* 34 (2019), pp. 196–208. DOI: 10.1016/j.ijdrr.2018.11.017.